Mechanism of replication machinery assembly as revealed by the DNA ligase–PCNA–DNA complex architecture

Kouta Mayanagi[a,b,1], Shinichi Kiyonari[c], Mihoko Saito[d], Tsuyoshi Shirai[d], Yoshizumi Ishino[c], and Kosuke Morikawa[b,e,1]

[a]Medical Institute of Bioregulation, Kyushu University, and Institute for Bioinformatics Research and Development, Japan Science and Technology Agency, 3-1-1 Maidashi, Higashi-ku, Fukuoka-shi, Fukuoka 812-8582, Japan; [c]Department of Genetic Resources Technology, Faculty of Agriculture, Kyushu University, and Institute for Bioinformatics Research and Development, Japan Science and Technology Agency, 6-10-1 Hakozaki, Higashi-ku, Fukuoka-shi, Fukuoka 812-8581, Japan; [d]Nagahama Institute of Bio-Science and Technology and Institute for Bioinformatics Research and Development, Japan Science and Technology Agency, 1266 Tamura-cho, Nagahama, Shiga 526-0829, Japan; [b]Institute for Protein Research, Osaka University, 6-2-3 Furuedai, Suita, Osaka 565-0874, Japan; and [e]Core Research for Evolutional Science and Technology, Japan Science and Technology Agency, Sanban-cho, Chiyoda-ku, Tokyo 102-0075, Japan

Edited by John Kuriyan, University of California, Berkeley, CA, and approved February 4, 2009 (received for review November 12, 2008)

The 3D structure of the ternary complex, consisting of DNA ligase, the proliferating cell nuclear antigen (PCNA) clamp, and DNA, was investigated by single-particle analysis. This report presents the structural view, where the crescent-shaped DNA ligase with 3 distinct domains surrounds the central DNA duplex, encircled by the closed PCNA ring, thus forming a double-layer structure with dual contacts between the 2 proteins. The relative orientations of the DNA ligase domains, which remarkably differ from those of the known crystal structures, suggest that a large domain rearrangement occurs upon ternary complex formation. A second contact was found between the PCNA ring and the middle adenylation domain of the DNA ligase. Notably, the map revealed a substantial DNA tilt from the PCNA ring axis. This structure allows us to propose a switching mechanism for the replication factors operating on the PCNA ring.

DNA replication | electron microscopy | single-particle analysis | DNA sliding clamp | protein-DNA complex

DNA ligase plays essential roles in various DNA transactions, such as joining Okazaki fragments in DNA replication and nick-sealing at the final step of several DNA repair pathways, including nucleotide excision repair, base excision repair, and mismatch repair (1, 2). The enzyme catalyzes phosphodiester bond formation at the nicks generated within dsDNA, through the well-conserved 3-step reaction using either NAD^+ or ATP as a cofactor (3). At the first step, the DNA ligase interacts with the nucleotide cofactor to form a covalent ligase–nucleoside monophosphate. At the second step, the bound AMP is transferred to the 5′ terminus of the DNA, and finally, a phosphodiester bond is formed by a reaction between the 5′-DNA-adenylate and the 3′-hydroxy group.

To date, 3 crystal structures of ATP-dependent eukaryotic-type DNA ligases have been reported. The structures of the 2 archaeal DNA ligases from *Pyrococcus furiosus* (PfuLig) and *Sulfolobus solfataricus* (SsoLig) were determined in the closed (4) and extended forms (5), respectively. The structure of the human DNA ligase 1 (hLigI) in complex with DNA (6) revealed that the enzyme entirely encircles the nicked DNA. All of these DNA ligases are in common composed of 3 domains, designated as the DNA binding domain (DBD), the adenylation domain (AdD), and the OB-fold domain (OBD), in the sequences from the N to C termini. Although the internal architectures of these domains are strikingly similar among the 3 DNA ligases, their relative domain orientations within each enzyme are quite different. Similar to many other replication factors, such as DNA polymerase and Flap endonuclease 1 (FEN1), DNA ligases exhibit the full activity by binding to proliferating cell nuclear antigen (PCNA). A small-angle X-ray scattering analysis revealed that the morphology of SsoLig in complex with PCNA coincides with the extended structure of SsoLig alone (5). However, the structure of the ternary Lig–PCNA–DNA complex remains unknown.

PCNA interacts with various protein factors to control DNA metabolism. It works not only as the platform for these factors on the DNA strand, but also as the conductor for the recruitment and release of these crucial players (7–9). These protein factors generally interact with the C-terminal and interdomain connecting loop (IDCL) of PCNA through the consensus sequence, which is called the PCNA binding protein box (PIP-box) (10) and is generally located at the N or C terminus. The hLigI protein also bears a PIP-box in the N-terminal domain (11, 12), whereas the corresponding domain is missing in archaeal DNA ligases. Recently, a functional PCNA binding motif of PfuLig, -QKSFF-, was found in a loop within the middle of the DBD, rather than the terminus of the enzyme (13).

The trimeric ring of the PCNA clamp can, in principle, provide at most 3 binding sites for each replication factor. The crystal structure of the human FEN1–PCNA complex indeed presented a view in which 3 FEN1 were bound in different orientations on a single PCNA clamp (14). A biochemical study of the *S. solfataricus* proteins supported the idea that 3 factors, such as DNA polymerase B1, FEN1, and DNA ligase, could simultaneously bind to a single PCNA clamp (15). It is an attractive idea to consider the "PCNA revolver" as the switching mechanism for each factor on the single PCNA ring to work sequentially. However, the actual view of this process remains unknown at the molecular level. Indeed, the clamp loading ternary complex revealed that the PCNA ring is almost completely covered by the RFC molecule, thus preventing interactions with other factors (16). The PCNA clamp and bacterial β clamp, which form trimeric and dimeric structures, respectively, exhibit very similar overall 3D structures with a pseudo 6-fold symmetry, despite their low sequence similarity to each other (17–20). Intriguingly, it was recently reported that the accommodated DNA is tilted by 22° from the ring axis in the bacterial clamp–DNA complex (21). In agreement with this finding, the molecular dynamics simulation indicated that the tilted DNA may play crucial roles in switching among the protein factors bound to the PCNA (22).

Author contributions: K. Mayanagi, Y.I., and K. Morikawa designed research; K. Mayanagi and S.K. performed research; K. Mayanagi, M.S., and T.S. analyzed data; and K. Mayanagi, S.K., T.S., Y.I., and K. Morikawa wrote the paper.

The authors declare no conflict of interest.

This article is a PNAS Direct Submission.

[1]To whom correspondence may be addressed. E-mail: maya@bioreg.kyushu-u.ac.jp or morikako@protein.osaka-u.ac.jp.

This article contains supporting information online at www.pnas.org/cgi/content/full/0811196106/DCSupplemental.

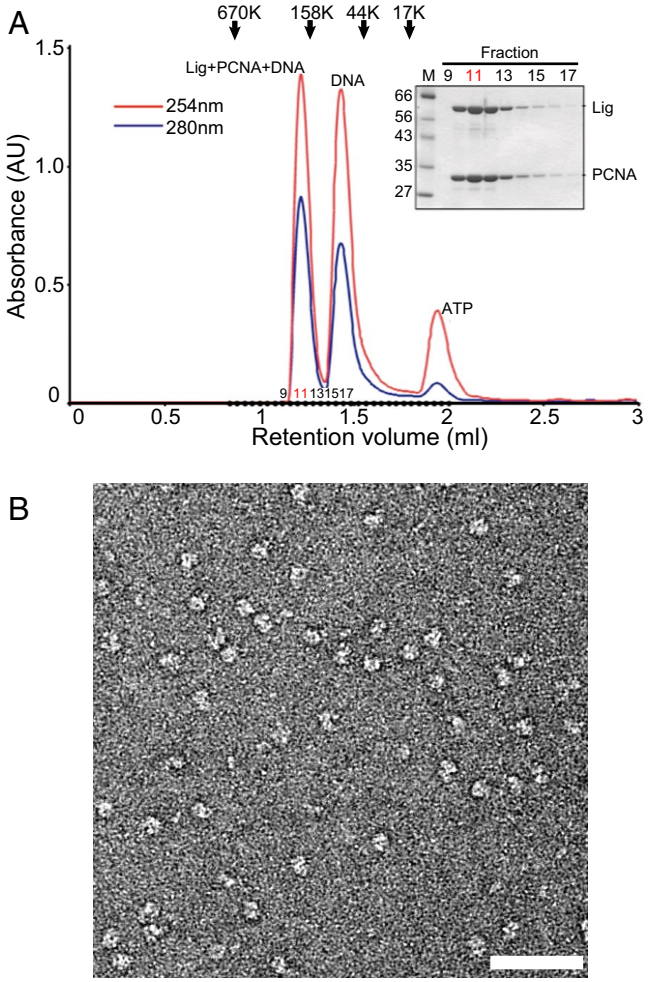

Fig. 1. Sample preparation and EM of the PfuLig–PCNA–DNA complex. (*A*) Isolation of the PfuLig–PCNA–DNA complex by gel filtration chromatography. Positions of the molecular mass standard markers are indicated on the top of the profiles. The fraction numbers and the lane numbers of SDS gel electrophoresis are equivalent to each other. Lane M: morecular mass markers. (*B*) Electron micrograph of the negatively-stained PfuLig–PCNA–DNA complex. (Scale bar: 50 nm.)

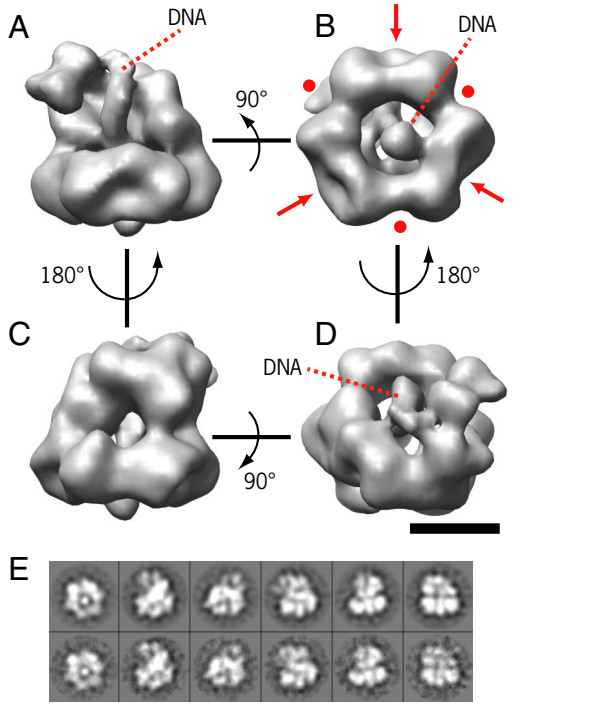

Fig. 2. 3D structure of the PfuLig–PCNA–DNA complex. (*A*) Front view. (*B*) Bottom view. The red dots and arrows indicate the concave edges and flat edges, respectively, of the PCNA ring with the pseudo 6-fold symmetry. (*C*) Back view. (*D*) Top view. (Scale bar: 5 nm.) (*E*) The reprojections of the 3D structure of the complex (*Upper*), with the corresponding 2D class averages (*Lower*). The side length of the individual images is 17.4 nm.

Here, we report the 3D structure of the PfuLig–PCNA–nicked DNA complex, which was obtained by EM single-particle analysis. We have successfully visualized the replication–relevant ternary complex, where the closed clamp complexed with the enzyme accommodates the substrate DNA. This complex structure also revealed a unique interaction between the DNA ligase and the clamp and allowed us to envision how the PCNA platform plays major roles in the sequential recruitment of replication factors into the replisome.

Results

EM and Overall Structure of the Complex. Using nonligatable, nicked DNA (a dideoxyribose at the 3′ terminus of the ligation site), we successfully stabilized the intermediate state of the DNA ligation, and thus isolated the PfuLig–PCNA–nicked DNA complex for structural analysis. The ternary complex eluted as a single peak in gel filtration chromatography. The molecular mass was estimated from the elution position to be ≈164 kDa, corresponding to the total mass of each protein (Lig: 63.8 k; PCNA: 28.0 k; DNA: 19.6 k) at a stoichiometry of 1:3:1 for PfuLig, PfuPCNA, and the nicked DNA (Fig. 1*A*). The EM images revealed that the particles were well-dispersed and exhibited various shapes, but were almost the same size (Fig. 1*B*). Together with the gel filtration profile, this result suggested that single-particle analysis of the complex would be very promising.

The final 3D map (Fig. 2) showed that the complex comprises mainly 2 regions, a lower hexagonal ring region, corresponding to the PCNA, and an upper crescent-shaped region, which extensively covers the lower ring. The edge length of the hexagon was ≈48 Å, and the diameter of the central channel was 35 Å. The center of the complex clearly showed the15-Å-thick rod-shaped structure, which should be assigned to the dsDNA, surrounded by both the ring and the crescent-shaped region. Based on the 0.5 criterion of the Fourier shell correlation, the resolution was estimated to be 15 Å (Fig. S1*A*).

The crystal structure of the PfuPCNA fits nicely into the lower hexagonal ring (Fig. 3*A*). This ring exhibited 3-fold symmetry, rather than genuine 6-fold symmetry, as characterized by the alternating flat and concave edges, corresponding to the IDCL (Figs. 2*B* and 3*A*, red arrows) and intersubunit interface (Figs. 2*B* and 3*A*, red dots), respectively. This observation was important to uniquely allocate the trimeric PfuPCNA crystal structure in the hexagonal ring. The quality of the EM map at the hexagonal ring region indicates that the assignments of the other areas are also reliable. The length of the rod density coincides with that of the 32-bp-long dsDNA, indicating that almost the entire length of the DNA is visualized (Fig. 3*B*).

Fitting of the Crystal Structures of DNA Ligases. The upper crescent region consisted of 3 domains, which all contacted the DNA rod (Figs. 2 and 3). The first 2 large domains contacted the PCNA hexagonal ring at 2 of the flat edges (IDCL). This finding was consistent with the characteristics of PCNA IDCL, which functions as a universal platform for various PCNA binding proteins. The third drooping domain, with a slightly smaller size, con-

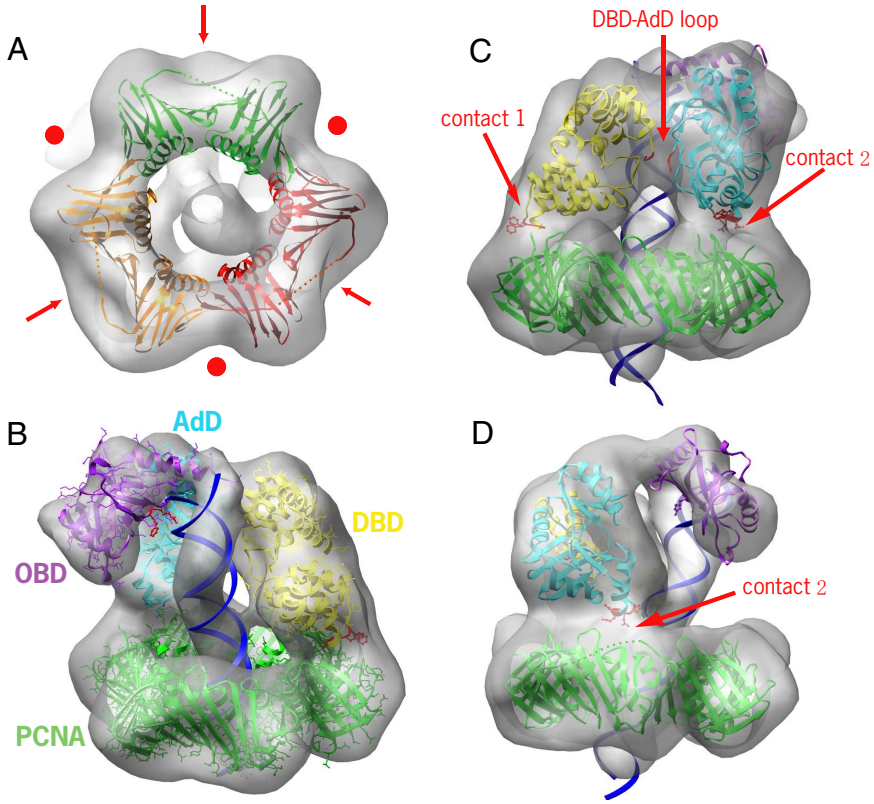

Fig. 3. Docking of the crystal structures of each component into the EM map of the ternary complex. (*A*) PfuPCNA crystal structure fitted to the EM map. The red dots and arrows indicate the intersubunit interfaces and interdomain connecting loop regions of the PCNA ring, respectively. The 3 PCNA subunits are displayed in green, orange, and red ribbon models to highlight the trimeric configuration of the PCNA clamp. The disordered regions of the IDCLs are shown by broken lines. (*B*) Oblique view of the complex. The crystal structures of PfuLig DBD (yellow), AdD (light blue), and OBD (purple) were docked independently into the map. The atomic models of PCNA and DNA are represented by green and blue ribbon models, respectively. The PCNA interacting -QKSFF- motif in DBD (red stick) and the DNA interacting residues Arg-523 and Phe-524 in OBD (red stick) are shown. (*C*) Back view of the complex. The 2 Lig–PCNA interactions are denoted by the red arrows and notations. Both ends of the DBD-AdD loop are colored red. The -QKSFF- motif in the contact 1 area and the AdD residues (His-323-Glu-326) near the contact 2 area are represented by red stick models. (*D*) Side view of the complex.

tacted the top of the DNA rod and the second domain. Notably, no interaction was observed between the third domain and PCNA.

Based on the overall shapes and sizes of the 3 domains, we could convincingly identify the first 2 large density regions in our EM map as the DBD and AdD, and the third drooping density as the OBD (Fig. 3*B*, denoted by DBD, AdD, and OBD). However, the relative orientations of each domain, particularly that of the OBD, were quite different from those in the crystals, and none of the 3 eukaryotic-type DNA ligase structures could be fitted as an intact molecule into the upper density region. The large discrepancy of the OBD orientation should be ascribed to the striking flexibility of the DNA ligase molecule (5), as proposed from the comparison of the 3 crystal structures from the human (6), *S. solfataricus* (5), and *P. furiosus* (4) proteins. These 3 structures indeed exhibited different OBD arrangements. Among the 3, SsoLig alone exhibited the stretched domain arrangement (5) (Fig. S2 *A* and *B*). The DNA-free PfuLig and hLigI in complex with DNA adopted the closed conformations, and both exhibited interactions between the N-terminal DBD and the C-terminal OBD. However, even these 2 closed conformations exhibited the pivot motion of OBD by nearly 180° (4, 6). In contrast to the OBD, the orientations between DBD and AdD were similar among the 3 crystals. Especially, the structures of the 2 archaeal DNA ligases fit nicely into the first 2 domains of the EM map (Fig. S2 *A* and *B*), although a better result was obtained when the loop between DBD and AdD was eliminated and then each domain was fitted independently (Fig. S3*A*). Although we did not assume any further restriction of the domain orientation when using the fitting tool of the Chimera program, the -QKSFF- motif (13) in the DBD was located close to the PCNA, and both ends of the cleaved DBD–AdD loop were close to each other, highlighting the reliability of the docking model.

Notably, AdD presents the second contact site between PfuLig and PCNA (Fig. 3 *C* and *D*). According to the docked atomic model of AdD, this contact site involves the loop (R321–N324) between helices A3 and A4 (the third and fourth helices of AdD), in addition to several residues at the N terminus of helix A4.

It appears that the discrepancy of the domain configuration between PfuLig and hLigI can be attributed to these 2 PfuLig–PfuPCNA contacts. The atomic model of hLigI in the human LigI–DNA crystal could not be docked into the EM map of the ternary complex, and the overlay of the DNA between our EM map and the hLigI–DNA crystal structure indicated that a considerable region of hLigI protrudes from the EM map (Fig. S2*C*). In the EM map of the ternary complex structure, the PfuLig winds about halfway around the DNA rod and does not completely enclose the DNA substrate, as seen in the hLigI–DNA complex (6). The domain configuration in the hLigI–DNA crystal is completely free from the restrictions of contacting PCNA, thus allowing the DNA ligase domains to encircle the DNA more tightly. A similar closed ligase structure, encircling the substrate DNA, was also observed in the chlorella virus DNA

ligase–DNA complex, which was crystallized in the absence of PCNA (23).

The DBD of PfuLig and hLigI consists of 2 triangular, prism-shaped subdomains (4, 6), which are connected through 2 loops (Fig. S3*B*) and referred to as the "terminal part" (helices I–III and X–XII) and the "middle part" (helices IV–IX) (4). The PCNA binding -QKSFF- motif is located in the middle part subdomain, which corresponds to the lower part of the DBD region in our EM map. In the fitting, the middle part subdomain could be best docked into the EM map, when the 2 linker loops between the 2 DBD subdomains were cut and the middle part subdomain was fitted independently (Fig. 3*C* and Fig. S3*A*). Thus, we obtained the entirely consistent model, where the -QKSFF- motif lies closer to the C terminus and IDCL of PCNA (Fig. 3 *B* and *C* and Fig. S3*A*). This improvement of the docking procedure seems to be reasonable, considering that a 25° kink motion in the DBD was observed between the PfuLig and hLigI crystal structures (4, 6).

Although the dockings of the DNA ligase domains and the PCNA subunits into our EM map were mostly straightforward, we found notable ambiguity in the docking of OBD, which might be caused by the poor quality of the density map in this area. Consistently, the orientations of the OBD were strikingly different among the 3 crystals, suggesting the high mobility of this domain (4–6). This unfixed location of the OBD was also highlighted from the crystal structures of smaller ATP-dependent DNA ligases (23, 24), which exhibited OBD orientations, not only different from our structure, but also from each other. Furthermore, in the EM map, this domain alone lacks contact with PCNA, whereas the DBD and AdD interact with PCNA. Thus, the final model was constructed, assuming that 2 basic residues, Arg-523 and Phe-524, corresponding to Arg-871 and Phe-872 involved in DNA binding in hLigI (6), should interact with the DNA (Fig. 3*B*).

DNA Interacts with the PCNA in a Tilted Configuration. An intriguing contact was observed between the DNA rod density and the inner wall of the hexagonal ring (Fig. 3*A*). This contact was consistently observed in all of the preliminary 3D maps, which were independently calculated by using different datasets and different initial reference 3D maps and refinement parameters (Fig. S1). Notably, the DNA did not pass perpendicularly to the PCNA plane, but was tilted by 16° from the PCNA 3-fold axis (Fig. 4).

The crystal structure of the bacterial β-clamp in complex with DNA clearly revealed that the DNA was tilted from the clamp axis and bound to the inner walls of the clamp channel on opposite sides (21). Within the clamp-loading complex, by contrast, the dsDNA runs perpendicularly to the PCNA plane and in parallel to the symmetrical axis and lacks apparent contacts with the PCNA (16). These results suggested that the actual DNA orientations in ternary complexes differ among the enzymes (DNA ligase in our case), that contact both DNA and PCNA, although the DNA in complex with PCNA alone may tilt by up to 20°, as predicted (22).

To identify potential amino acid residues involved in the DNA contact, we aligned the crystal structure of PfuPCNA with that of the *Escherichia coli* β-clamp complexed with DNA. The 2 structures superimposed well (90% structural overlap, rmsd = 3.7 Å), despite their low sequence identity (12%). The β-clamp–DNA complex structure revealed that residues N15, R24, R73, R80, H148, N149, and R205 are involved in DNA binding. The alignment allowed us to predict that PfuPCNA residues K209 (for β-clamp R205), H75 (for K198), K77, K78, and K81 (for R80 or R205) correspond to these key residues (Fig. S4). Intriguingly, K209 and K81 lie very close to the DNA–PCNA contact region in the EM map (Fig. 4), suggesting that the interfaces of the clamps with DNA may be conserved among bacteria, archaea, and eukaryotes.

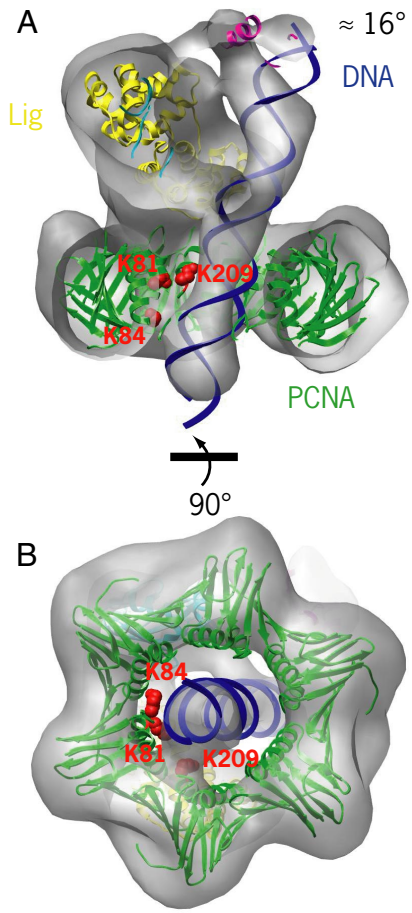

Fig. 4. Cross-section of the EM map of the complex showing the tilted DNA in contact with the inner wall of the PCNA. (*A*) Side view. (*B*) Bottom view. The key lysine residues K81 and K209 (red sphere) for the PCNA–DNA interaction, predicted from the crystal structure of the β clamp–DNA complex and the sequence alignment of the β-clamp and PCNA, are labeled in red notation, together with K84, which was also found close to the PCNA–DNA contact.

Discussion

DNA replication, repair, and cell cycle control involve various proteins that interact with PCNA. Therefore, PCNA not merely serves as a platform for DNA, but also coordinates PCNA binding proteins to cooperatively function in the above cellular processes, although the precise mechanism is still unknown (7, 8). Our ternary complex structure could provide important clues to understanding the switching mechanism of PCNA binding proteins operating on DNA.

Based on our structural model, we considered a mechanism in which these partners are bound and released sequentially. In fact, most of the PCNA binding proteins share the same binding sites, such as IDCL and the C-terminal tail of the PCNA. Our structural features exclude the possibility that the 3 protein factors contact the single PCNA ring at the same time, because DNA ligase occupies 2 of the 3 subunits of the PCNA trimer. Likewise, in the RFC–PCNA–DNA complex, RFC entirely covers the PCNA ring, thus blocking the entry of other protein factors (16). Collectively, our ternary complex, containing DNA ligase, appears to favor a mechanism involving the sequential binding and release of replication factors, as schematically represented in Fig. 5. In solution, a DNA ligase can adopt various

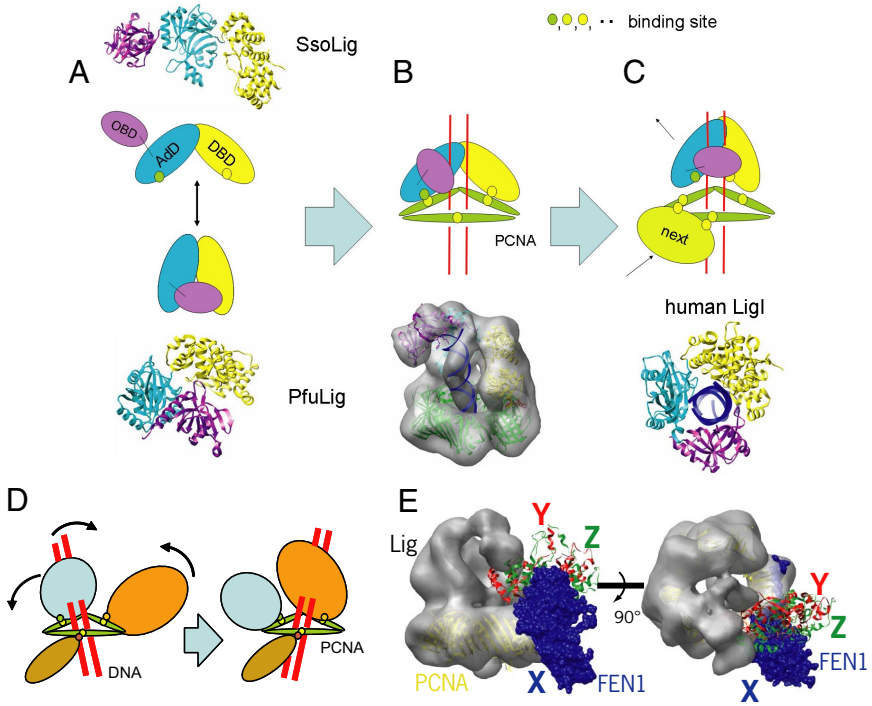

Fig. 5. Switching mechanism of PCNA binding factors. (*A*–*C*) Model switching mechanism proposed in this work. (*A*) In solution, the DNA ligase adopts various conformations, such as the closed and extended configurations, as observed in the PfuLig and SsoLig crystal structures, respectively. (*B*) Upon binding to PCNA and DNA, the DNA ligase forms the intermediate crescent configuration, which embraces the DNA. (*C*) The DNA ligase grips the DNA to accomplish the ligation of nicked DNA, as observed in the crystal structure of hLigI–DNA. Accordingly, the binding sites will be released, thereby enabling the PCNA ring to interact with the PIP-box of the next enzyme. (*D*) Switching induced by the DNA tilt and swinging-in and -out of the factors bound on the PCNA revolver, proposed in previous works (14, 15, 21, 22). (*E*) FEN1–PCNA crystal structure, superimposed on the EM map. FEN1 in the X (blue), Y (red), and Z (green) configurations, placed on the free IDCL region of PCNA (yellow).

conformations between the extended (5) and closed (4) forms (Fig. 5*A*). Our ternary structure could be regarded as an intermediate state, just before DNA ligation. Under the constraints within the ternary complex, the interaction with the DNA and PCNA would modulate the domain configuration of the DNA ligase molecule relative to PCNA, thereby inducing the kink motion within the DBD. This motion would generate the intermediate state, in which the DNA ligase forms the crescent configuration, embracing the DNA (Fig. 5*B*). The intermediate state, sustained through the bipartite interactions with PCNA, may explain the inhibitory effect of PCNA on ligation, as reported (25). When DNA ligase catalyzes the ligation reaction, tight binding between the enzyme and the substrate DNA, as revealed by the hLigI–DNA complex crystal structure (6), is required. Thus, it is not surprising that the conformation of DNA ligase complexed with DNA is distinct from that within our ternary complex. It is intriguing to consider that 1 of the 2 contacts, most possibly at the weaker AdD–PCNA contact site rather than that with the -QKSFF- motif, would be free in the ligase reaction, allowing the next factor (e.g., RFC for the clamp unloading) to interact with the PCNA ring through its PIP-box (Fig. 5*C*). Furthermore, the ternary complex structure may even allow us to envision that the extensive DNA ligase–PCNA contact could block the entry of other PCNA binding proteins. The structure also implies that the ligation reaction would be coupled with the dissociation of DNA ligase from PCNA, thereby ensuring the correct order of various reactions in the replication factory.

Alternatively, we can consider the flip-flop transition mechanism, which enables protein factors to internally switch for different functions on the same DNA clamp (Fig. 5*D*). Intriguingly, the *S. solfataricus* PCNA heterotrimer binds FEN1, DNA ligase, and DNA polymerase simultaneously on each subunit of PCNA (15), implying that a flip-flop transition mechanism may occur among these replication factors. Consistent with this idea, the crystal structure of the human FEN1–PCNA complex (14) revealed that 3 FEN1s are bound to the single PCNA ring, in different configurations. The crystal structure of the β-clamp–DNA complex (21) also allowed the authors to propose an intriguing model, in which the 2 DNA polymerases (Pol III and Pol IV) bound to the same clamp ring can switch with each other, in response to alternate tilting movements of the DNA duplex accommodated within the clamp.

To test this model, we superimposed our ternary complex model onto the FEN1–PCNA crystal structure (14) (Fig. 5*E*). The fitting of PCNA in the FEN1–PCNA crystal structure into our 3D map revealed that the third binding site of PCNA was completely open for the FEN1 interaction, and that the globular domain of FEN1 in the X configuration did not clash with the DNA ligase. Meanwhile, a slight collision was observed between Lig OBD and FEN1 in the Y or Z configuration. However, when considering the positional flexibility of OBD, its rearrangement would allow FEN1 to adopt the Y and Z configurations as well.

Taken together, it is possible that the protein factors on the DNA clamp in vivo adopt several switching mechanisms, including the 2 models discussed above. Our structural study of the PfuLig–PCNA–DNA complex revealed that the architectures of the DNA and the protein factors on the DNA clamp are strikingly versatile in different functional states. In particular, considering previous findings (16, 21, 22), the orientations of DNA duplexes could broadly vary, depending on the protein factors bound to PCNA. Presumably, this versatile architecture would facilitate the functional switching between different proteins.

Experimental Procedures

EM and Single-Particle Image Analysis. The PfuLig and PfuPCNA were prepared as described (20, 26). The substrate DNA used in the sample preparation was a 32-bp DNA duplex containing a single nick. The 19-mer deoxynucleotide (5′-GCTTCTGTGCTGATGCGTddC-3′) and the 13-mer deoxynucleotide (5′-pGTCGGACTGAACC-3′) were annealed to the 32-mer deoxyoligonucleotide with a complementary sequence, in 40 mM Tris acetate (pH 7.8) and 0.5 mM magnesium acetate. The purified PfuLig (10 μM) and PfuPCNA (30 μM) were incubated with the nicked DNA substrate (10 μM) in 70 μL of ligation buffer, containing 20 mM Mes (pH 6.5), 10 mM $MgCl_2$, 50 mM NaCl, 0.1 mM ATP, and 0.1% Tween 20, at 50 °C for 15 min. The mixture was incubated at 20 °C for 15 min and was subsequently loaded onto a gel filtration column (Superdex 200 PC 3.2-30; GE Healthcare) equilibrated with elution buffer [20 mM Mes (pH 6.5), 10 mM $MgCl_2$, and 50 mM NaCl]. The fractions corresponding to the reconstructed complex were confirmed by SDS/PAGE.

A 3-μL aliquot of sample solution was applied to a copper grid supporting a continuous thin-carbon film, left for 1 min, and then stained with 3 drops of 2% uranyl acetate. Images were recorded by a BioScan CCD camera (Gatan) with a pixel size of 5.1 Å/pixel or 3.1 Å/pixel, using a JEM1010 electron microscope (JEOL) operated at an accelerating voltage of 100 kV. The magnification of the images was calibrated by using tobacco mosaic virus as a reference sample. A minimum dose system was used to reduce the electron radiation damage of the sample.

A total of 7,480 images of PfuLig–Pfu PCNA-nicked DNA (lig–PCNA–DNA) were selected by using the BOXER program in EMAN (27). Alignment, classification, and averaging of the particle images were performed by using the image analysis tools in IMAGIC (28). The initial 3D model was obtained from images taken with a pixel size of 5.1 Å/pixel, using the common-line method. Subsequent iterative alignment and 3D reconstruction were performed by using the REFINE routine in EMAN. The final model was obtained by performing the refinement procedure with the dataset (19,544 particles) recorded with a pixel size of 3.1 Å/pixel, starting from the 5.1 Å/pixel 3D model as the initial reference (Fig. S1*B*). The visualization of the 3D map and the fitting of the crystal structures into the map were performed with Chimera software (29). The crystal structure of PfuLig [Protein Data Bank (PDB) ID code 2CFM] was divided into 3 parts, residues 1–220 (DBD), residues 221–423 (AdD), and residues 424–561 (OBD), and docked independently to the obtained map, using the Fit Model in Map tool in Chimera. The middle part of DBD, corresponding to the residues 62–159, was further isolated from the DBD, and a better fit was searched for this subdomain, using the same tool.

Structural Alignment of the β-Clamp and PCNA. The structures of the *E. coli* β-subunit (PDB ID code 2POL) and *P. furiosus* PCNA (PDB ID code 1GE8) were superposed, to compare the DNA-binding sites. The β-subunit has 3 domains (N′-M′-C′), and 2 subunits, A and B, in the asymmetric unit constitute the clamp. The asymmetric unit of the PCNA crystal contains 1 subunit with 2 domains (N′-C′). The trimeric ring of PCNA was constructed by referring to the crystal symmetry. Every permutation of the domains was examined for ring superposition, because the domain compositions were different between the 2 proteins. The best similarity in the DNA-binding sites was observed when the β-subunit domains AN′-AM′-AC′-BN′-BM′-BC′ were superposed on the PCNA domains 1N′-1C′-2N′-2C′-N3′-3C′, respectively (Fig. S4).

ACKNOWLEDGMENTS. We thank H. Nishida for helpful discussions. This work was supported by the Institute for Bioinformatics Research and Development, Japan Science and Technology Agency. K. Morikawa was supported by the Core Research for Evolutional Science and Research, Japan Science and Technology Agency.

1. Tomkinson AE, Vijayakumar S, Pascal JM, Ellenberger T (2006) DNA ligases: Structure, reaction mechanism, and function. *Chem Rev* 106:687–699.
2. Ellenberger T, Tomkinson AE (2008) Eukaryotic DNA ligases: Structural and functional insights. *Annu Rev Biochem* 77:313–338.
3. Lehman IR (1974) DNA ligase: Structure, mechanism, and function. *Science* 186:790–797.
4. Nishida H, Kiyonari S, Ishino Y, Morikawa K (2006) The closed structure of an archaeal DNA ligase from *Pyrococcus furiosus*. *J Mol Biol* 360:956–967.
5. Pascal JM, et al. (2006) A flexible interface between DNA ligase and PCNA supports conformational switching and efficient ligation of DNA. *Mol Cell* 24:279–291.
6. Pascal JM, O'Brien PJ, Tomkinson AE, Ellenberger T (2004) Human DNA ligase I completely encircles and partially unwinds nicked DNA. *Nature* 432:473–478.
7. Moldovan GL, Pfander B, Jentsch S (2007) PCNA, the maestro of the replication fork. *Cell* 129:665–679.
8. Maga G, Hubscher U (2003) Proliferating cell nuclear antigen (PCNA): A dancer with many partners. *J Cell Sci* 116:3051–3060.
9. Vivona JB, Kelman Z (2003) The diverse spectrum of sliding clamp interacting proteins. *FEBS Lett* 546:167–172, 2003.
10. Warbrick E (1998) PCNA binding through a conserved motif. *BioEssays* 20:195–199.
11. Levin DS, Bai W, Yao N, O'Donnell M, Tomkinson AE (1997) An interaction between DNA ligase I and proliferating cell nuclear antigen: Implications for Okazaki fragment synthesis and joining. *Proc Natl Acad Sci USA* 94:12863–12868.
12. Montecucco A, et al. (1998) DNA ligase I is recruited to sites of DNA replication by an interaction with proliferating cell nuclear antigen: Identification of a common targeting mechanism for the assembly of replication factories. *EMBO J* 17:3786–3795.
13. Kiyonari S, Takayama K, Nishida H, Ishino Y (2006) Identification of a novel binding motif in *Pyrococcus furiosus* DNA ligase for the functional interaction with proliferating cell nuclear antigen. *J Biol Chem* 281:28023–28032.
14. Sakurai S, et al. (2005) Structural basis for recruitment of human flap endonuclease 1 to PCNA. *EMBO J* 24:683–693.
15. Dionne I, Nookala RK, Jackson SP, Doherty AJ, Bell SD (2003) A heterotrimeric PCNA in the hyperthermophilic archaeon *Sulfolobus solfataricus*. *Mol Cell* 11:275–282.
16. Miyata T, et al. (2005) Open clamp structure in the clamp-loading complex visualized by electron microscopic image analysis. *Proc Natl Acad Sci USA* 102:13795–13800.
17. Kong XP, Onrust R, O'Donnell M, Kuriyan J (1992) Three-dimensional structure of the β-subunit of *E. coli* DNA polymerase III holoenzyme: A sliding DNA clamp. *Cell* 69:425–437.
18. Krishna TS, Kong XP, Gary S, Burgers PM, Kuriyan J (1994) Crystal structure of the eukaryotic DNA polymerase processivity factor PCNA. *Cell* 79:1233–1243.
19. Gulbis JM, Kelman Z, Hurwitz J, O'Donnell M, Kuriyan J (1996) Structure of the C-terminal region of p21(WAF1/CIP1) complexed with human PCNA. *Cell* 87:297–306.
20. Matsumiya S, Ishino Y, Morikawa K (2001) Crystal structure of an archaeal DNA sliding clamp: Proliferating cell nuclear antigen from *Pyrococcus furiosus*. *Protein Sci* 10:17–23.
21. Georgescu RE, et al. (2008) Structure of a sliding clamp on DNA. *Cell* 132:43–54.
22. Ivanov I, Chapados BR, McCammon JA, Tainer JA (2006) Proliferating cell nuclear antigen loaded onto double-stranded DNA: Dynamics, minor groove interactions, and functional implications. *Nucleic Acids Res* 34:6023–6033.
23. Nair PA, et al. (2007) Structural basis for nick recognition by a minimal pluripotent DNA ligase. *Nat Struct Mol Biol* 14:770–778.
24. Subramanya HS, Doherty AJ, Ashford SR, Wigley DB (1996) Crystal structure of an ATP-dependent DNA ligase from bacteriophage T7. *Cell* 85:607–615.
25. Jonsson ZO, Hindges R, Hubscher U (1998) Regulation of DNA replication and repair proteins through interaction with the front side of proliferating cell nuclear antigen. *EMBO J* 17:2412–2425.
26. Nishida H, Tsuchiya D, Ishino Y, Morikawa K (2005) Overexpression, purification, and crystallization of an archaeal DNA ligase from *Pyrococcus furiosus*. *Acta Crystallogr F* 61:1100–1102.
27. Ludtke SJ, Baldwin PR, Chiu W (1999) EMAN: Semiautomated software for high-resolution single-particle reconstructions. *J Struct Biol* 128:82–97.
28. van Heel M, Harauz G, Orlova EV, Schmidt R, Schatz M (1996) A new generation of the IMAGIC image processing system. *J Struct Biol* 116:17–24.
29. Pettersen EF, et al. (2004) UCSF Chimera: A visualization system for exploratory research and analysis. *J Comput Chem* 25:1605–1612.